110th Anniversary

Wood, Thomas; Simmons, Mark John H.; Greenwood, Richard W.; Turnbull, Stephanie A; Stitt, E. Hugh

DOI:
10.1021/acs.iecr.9b00572

110th Anniversary:

Slurryability: What makes a powder hard to incorporate into a slurry?

Thomas Wood[a,b], Mark J. H. Simmons[b], Richard W. Greenwood[b], Stephanie A. Turnbull[a], E. Hugh Stitt[a*]

[a]* *Johnson Matthey Technology Centre, P.O. Box 1, Belasis Avenue, Billingham, TS23 1LB*

[b] *School of Chemical Engineering, University of Birmingham, Birmingham B15 2TT, UK*

*hHugh. sStitt@mMatthey.com

Abstract

This paper investigates powder properties that are significant in determining how easily a powder may be incorporated into water to form a concentrated slurry. The slurryability of a powder is defined as the time and energy required to prepare a 50 wt% slurry, as well as a threshold concentration at which it requires 1 kJ to further increase the solid content by 1 wt% at the scale studied.

Partial least squares (PLS) models relating powder properties to their slurryability are built on a dataset of thirteen powders. The most significant properties determining slurryability are the particle pore volume, powder bulk density, and the results of permeability and aeration tests on a powder rheometer. The d_{50} particle size and powder cohesion measurements are also relevant in the models.

By measuring only these six properties the slurryability of two further powders, not included in the training dataset, were predicted within ±10 %.

Formatted: Font: Bold

Field Code Changed

Introduction

Throughout the process industries there is often a dichotomy between the formulation development and manufacturing stages of delivering a new product. This leads to issues with the 'manufacturability' of a new product as it moves from the laboratory scale into newly designed or existing manufacturing plants. This is inefficient, as useful data are either lost or not recorded during the formulation stage, which could be invaluable to the improvement and development of manufacturing processes. It can also be costly as new products may be sent to manufacture before they can be successfully made, either requiring extra development work or compromises in product quality or manufacturing cost. *In extremis*, the process may even fail due to unpredicted effects of manufacturing at scale. Such products can include concentrated high solids content slurries, created by the addition of large amounts of powdered solid (up to and above 50 wt%) to liquid media in a stirred vessel; these arise in a wide range of industries including paint[1], catalyst[2], consumer goods[3] and aerospace[4].

Previously, an optimised geometry was designed to maximise the efficiency of powder incorporation to prepare concentrated slurries at laboratory and larger scales[5,6]. However, it was noted that the scale up of this geometry was strongly affected by a step-change in incorporation performance that occurred at approximately 40 wt% for the alumina studied. This value of 40 wt% was observed to be specific to the type of powder studied and thus may be considered a powder characteristic for an individual liquid. This study considers a wide range of different powders and uses multivariate statistical modelling to determine which powder properties drive the point at which this transition occurs: this should enable the prediction of this transition based on characterisation of new powders. The ease with which powders are incorporated, defined by how concentrated it is possible to make a slurry before reaching this transition, is referred to here as the *slurryability* of that powder. Raw material properties can significantly impact the behaviour of those materials through

a manufacturing process[7,8]. However, there are no previous studies considering the effect of raw powder properties on their ease of incorporation into high solids content dispersions.

The concentration of a slurry has so far been referred to on a wt/wt basis. This is generally how formulations involving powders are specified, weight being a considerably more reliable measure for powder quantity than volume, which is dependent upon the previous handling of the powder[9–11]. However, volume concentration has been shown to be a better predictor of the slurry rheology, and therefore the effect of the powder on the behaviour of the system[12].

The flow behaviour of fine powders is not trivial, with multiple measurements being required to characterise powders sufficiently for even simple design calculations[13]. In this study the powder is added to water to prepare a slurry. This adds further complication to the forces acting on individual particles. Due to the presence of three phases at the liquid surface, the interfacial tension between the liquid and the solid has a significant effect on the complex force balance on the solid. This value of the interfacial tension is specific to combination of the individual powder and liquid being studied and can give dramatically different powder wettability behaviour if different liquids or solids are studied[14]. In highly hydrophobic solids the high interfacial tension with water can prevent particles from becoming wetted and thus being fully incorporated[15]. It can also promote agglomeration of particles, where air becomes trapped within the agglomerate giving it a lower bulk density than the solid density, causing it to float even if the solid would sink. The formation of semi-wetted agglomerates may also lead to an increase in the apparent volume fraction of the dispersed phase, with resulting impact on the suspension rheology. This strong impact of wettability on the behaviour of particles in a solid-liquid system makes it a key parameter in many sectors. Examples where this is true include the pharmaceutical sector[16] and the food and personal care industries where the interfacial tension of solids used to stabilise colloidal interfaces is important[17–19]. The wettability of a solid is generally indicated as the three-phase contact angle between the solid, liquid, and air given by Young's equation and shown in equation 1[20]:

$$\gamma_{SL} = \gamma_{SV} - \gamma_{LV}\cos(\theta) \#(1)$$

Where θ is the three phase contact angle and γ is the interfacial tension between two phases, denoted as solid (S), liquid (L), and vapour (V).

This contact angle can be measured through several methods depending on the size and shape of the solid being studied and can generally be classified into three distinct categories: sessile drop, capillary rise, and direct measurement of the interfacial tension. This last category involves use of microcalorimetry[21] or inverse gas chromatography[22]; expensive techniques that would only be available in a specialist research group or facility. Capillary rise methods, based on measuring the uptake of fluid through a powder bed with time, can be used to measure the contact angle through application of the Washburn equation[23]:

$$h^2 = \bar{r}\frac{\gamma_{LV}\cos(\theta)}{2\mu}t \#(2)$$

Where h is the liquid height at time t, μ is the liquid dynamic viscosity, and $\bar{r}$ is the mean capillary radius. This approach is used frequently for a wide variety of powders[24–26]. However, researchers have reported issues when studying powders comprised of porous particles, demonstrating irreproducible results and effects of the particle porosity and shape on the liquid rise through the bed[2,24,27,28].

Sessile drop methods involve placement of a liquid drop onto the liquid surface and directly measuring the angle between the solid and the liquid using a camera. This is simple for flat solids. However, it presents problems for powders, which do not present a flat surface and so the observed contact angle may not be the actual contact angle, as powder between the droplet and the camera can obscure the true measurement[29]. Nowak *et al*[28] compared various capillary rise and sessile drop approaches for measurement of the three phase contact angle for highly porous solids and found that the most consistent method involved placing a sessile drop onto a thin layer of powder dispersed onto a glass slide.

Two multivariate data analysis tools are used in this study. The first, principle component analysis (PCA), first developed by Karl Pearson in 1901[30] is a tool used to reduce the dimensionality of a dataset. It is used herein as a data exploration tool to find powders with similar behaviour and to map the relationships between various powder properties and powder slurryability. PCA is frequently used in a wide variety of fields including stock market analysis and prediction in the finance sector[31], image processing[32], and pharmaceutical formulation development[33]. Wang *et al*[34] used PCA to study the effect of powder properties on the performance of a loss in weight powder feed system.

Partial least squares regression modelling (henceforth referred to as PLS) is a powerful multivariate statistical technique that looks for underlying latent structures within two datasets, a predictor dataset (X) and a response dataset (Y). A linear regression model is used to predict the maximum multidimensional variance in the Y space, explained by a multidimensional direction in the X space[35]. PLS has found particular use in the field of chemometrics for spectral calibrations[36–38], where the ability of PLS to comfortably deal with highly co-correlated X variables (such as spectral bands) and more variables than observations make it a highly useful tool for building calibrations[35]. More recently PLS is finding more use in study of process data, finding complex multivariate relationships between process and recipe formulation variables[39,40]. There are multiple ways to consider the relative effects of different variables in the X space in PLS models. One of the simplest is the use of Variable Importance in the Projection (VIP) scores, which are defined in equation 3[41].

$$VIP_i = \sqrt{d\frac{\sum_{k=1}^{h} \nu_k(\omega_{ki})^2}{\sum_{k=1}^{h} \nu_k}} \quad (3)$$

Where d is the number of variables, h is the number of latent variables in the PLS model, ν_k is the fraction of explained variance in the X space by latent variable k, and ω_{ki} is covariance weighting for each variable, i, over all latent variables. A cut off threshold is often used for VIP scores, where a variable with VIP scores < 1 is deemed insignificant[41].

This study defines a measure to compare slurryability between a number of different powders. By measurement of a wide range of powder properties, PLS is used to build a predictive model for the slurryability of powders based on their bulk and particle properties. This model is validated through two additional powders which were not part of the datasets used to build the model. VIP scores are also used to find the most important powder properties dictating the slurryability of a given powder.

Materials and Methods

Materials

In this study 15 different commercially available porous and non-porous powders were studied to build and test the predictive multivariate models used. Thirteen of these were used to build the statistical model, listed in Table 1. The data from remaining two were used to test and validate the model. The powders were characterised by a variety of techniques which are described below.

Table 1: List of materials studied

Powder Name	d_{10} (µm)	d_{50} (µm)	d_{90} (µm)	Skeletal density (kg m^{-3})	Poured density (kg m^{-3})	Tapped density (kg m^{-3})	Mean pore size (A)	Pore volume ($cm^3 g^{-1}$)
Mixed oxide 1	7.65	25.10	57.30	2432	909	1109	206	0.321
γ-alumina 1	4.02	18.80	39.30	3352	662	793	107	0.415
α-alumina 1	11.80	116.00	245.00	2701	313	381	345	1.53
α-alumina 2	13.50	69.50	147.00	2688	465	567	271	0.78
Stabilised γ-alumina 1	3.20	21.00	62.40	2731	380	498	181	0.7014
Titania	0.03	0.96	3.00	3900	247	357	0	0
Magnesia 1	2.02	15.46	31.21	3580	651	883	307	0.241
Magnesia 2	1.98	16.42	33.12	3620	510	690	318	0.251
Glass frit 1	0.40	3.00	479.60	5389	1124	1337	0	0
Mixed oxide 2	3.31	15.01	30.20	6130	1100	1210	289	0.285
Zeolite	1.99	5.02	10.89	2210	450	570	150	0.416
γ-alumina 2	0.81	2.01	21.12	2698	492	679	68	0.147
γ-alumina 3	6.12	47.23	187.65	2701	736	879	71	0.358

Powder Characterisation

Particle size was measured by laser diffraction using a Malvern Mastersizer 3000 (Malvern Instruments, UK) using a dry dispersion module. The results are reported as D_{10}, D_{50} and D_{90} which represent the size at which 10 %, 50 %, and 90 % respectively of the solid volume in the powder sample is comprised of particles with an equal or lesser volume than a sphere of that diameter.

Multiple density terms are considered as no individual definition of density can describe all the necessary features of an individual powdered solid. The first density measurements considered are the poured and tapped bulk density measurements, bulk powder density values measured using a measuring cylinder with a known mass of powder carefully poured into it to give the poured density. This cylinder is then tapped 2000 times using a Tapped Density Tester (Copley Scientific, UK). These were used to calculate the Hausner ratio, H, (equation 4) [11] and Carrs Index, C, (equation 5) [9] as:

$$H = \frac{\rho_T}{\rho_B} \#(4)$$

$$C = 100\left(1 - \frac{\rho_B}{\rho_T}\right) \#(5)$$

These values are often used as rule of thumb metrics to determine the flowability of a powder, with HR values > 1.25 and CI values > 25 indicating poor flow. These values are clearly related and will show a significant degree of co-correlation. However, this is easily handled by the multivariate statistical approaches used in this study so there is little reason to neglect either.

Skeletal density measurements, a measure of the density of the pure solid material, neglecting inter- and intra- particle pores, were taken using helium pycnometry. Mean pore diameters and pore volumes were measured using nitrogen adsorption BET.

Powder Flow Characterisation

Powder flow characterisation was carried out in two different types of equipment: a shear cell for quasi-static behaviour and a powder rheometer for dynamic characterisation. The rheometer was

used also to assess powder aeration and compressibility as well as permeability of a compact powder bed.

Shear Cell

A Brookfield Powder Flow Tester (PFT) (AMETEK Brookfield, USA) was used to perform shear cell measurements on the powders. The test consists of three steps: (1) pre-compaction of a pre-prepared uniform powder bed to an initial consolidation stress, (2) the powder is sheared until a steady state is achieved, this is the preshear point, (3) the normal stress is then reduced and the yield point is again found by applying a shear stress to the powder bed. This is repeated for five normal stresses to give a yield locus, as shown in Figure 1[42]. This test is repeated at normal consolidation stresses of 15 kPa, 9 kPa, 6 kPa, and 3 kPa to give four yield loci.

A Mohr-Coulomb analysis approach is used, where a linear regression is fitted to the yield locus. The slope of this linear regression, ϕ, is an estimate of the powder internal angle of friction. Two Mohr circles are used to find the flow function of the powder. The first of which passes through the origin and is tangential to the yield locus defines the powder unconfined yield strength, σ_c, as shown in Figure 1[42]. The second Mohr circle is drawn tangential to the yield locus at the preshear point and defines the major principal stress, σ_1. The powder flow function (ffc) is defined as the gradient of a plot of the major principal stress against the unconfined yield strength. Figure 2 shows a guideline of how the flow function of a powder corresponds to how easily it is likely to flow.

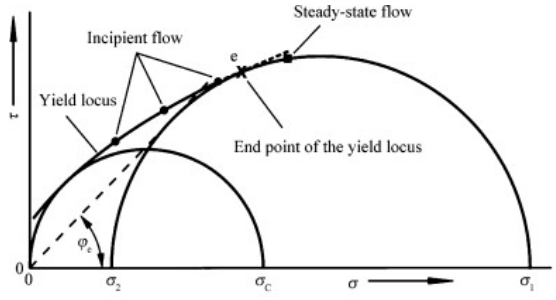

Figure 1: Example yield locus of a powder bed [42]

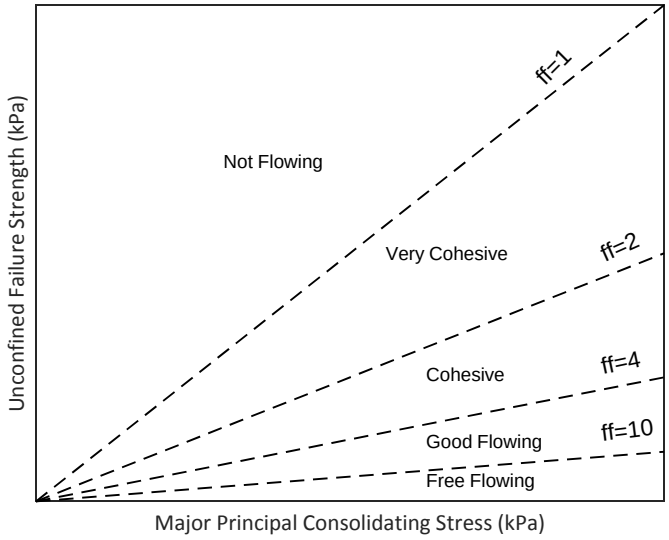

Figure 2: Guideline flow function values for different powder flow regimes

Freeman FT4 Powder Rheometer

A series of tests were carried out on a Freeman FT4 powder rheometer (Freeman Technologies, UK). For each test the powder is first conditioned in the rheometer by a helical blade, shown in Figure 3, moving up and down through the powder bed three times at a tip speed of 60 mm s^{-1} to give a uniform powder bed and to remove the handling history of the powder[43]. Four different tests are carried out in the FT4, all of which are preceded by this conditioning stage: the compressibility test, the permeability test, the flow energy test, and the aeration test.

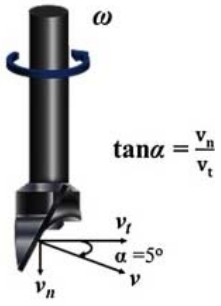

Figure 3: Freeman FT4 powder rheometer helical impeller blade used for conditioning and measurement

In the compressibility test the powder is subjected to a normal pressure up to 15 kPa for one minute. The powder compressibility is given as a function of the change in powder bed volume:

$$C\ (\%) = 100\frac{V_i - V_C}{V_i}\ \#(6)$$

Where V_i is the powder volume after conditioning and V_C is the compressed powder volume.

In the permeability test air is passed through the powder bed after the conditioning step at a flow rate of 2 mm s^{-1}. The powder bed is compressed at 15 kPa during this test. The permeability of the powder is indicated by the measured pressure drop across the powder bed, with a low pressure drop indicating a high permeability powder bed. The permeability of a powder bed is proportional to the bed porosity and particle diameter squared using Darcy's law and the Kozeny-Carman equation respectively[44,45].

In the basic flow energy dynamic test the powder is initially conditioned. Following this the impeller is passed down through the powder bed at a fixed velocity. The energy required for the powder to flow during this test is measured by the torque on the impeller and the normal force exerted on the base of the instrument. Higher flow energies indicate a higher level of mechanical locking and friction, this would indicate powders with higher angles of internal friction that are less likely to flow easily. This test is repeated three times with a conditioning stage in between each measurement.

The aeration test is similar to the basic flow energy test. In this test the powder is fluidised where possible, if not it is simply aerated, and the normal dynamic test is carried out. The test is repeated three times at air flows decreasing from 20 mm s^{-1} to 0 mm s^{-1}. At each air velocity the flow energy is measured three times, with a conditioning stage between each measurement. The aeration index is the ratio of flow energy under fixed bed conditions[46], i.e. air velocity = 0 mm s^{-1}, and the flow energy under full fluidisation where possible, or at 20 mm s^{-1} where the powder will not fluidise. This measurement is used to give an indication of how the powder behaves when aerated, with high

aeration indexes suggesting that the powder is easily aeratable and does not remain cohesive whilst aerated, allowing the impeller blade to easily move through the bed.

Powder Wetting Characterisation

Contact Angle

To measure the powder contact angle with water the method shown by Nowak *et al*[28] to be most appropriate for use with highly porous powders was used. A thin layer of powder was adhered to a flat surface using a spray adhesive. Particles not firmly attached to the slide 30 seconds after application were removed. The size of the liquid drop was chosen such that the mean capillary length, a, defined in equation 7, was larger than the radius of the droplet. This is done to make the effect of gravity negligible when compared to capillary effects[47]. The capillary length of water is 2.7 mm so a 10 µL droplet was used for all solids, giving a droplet with radius approximately 2.3 mm[48].

$$a = \sqrt{\frac{2\lambda}{\rho g}} \#(7)$$

A KRUSS Drop Shape Analyser (DSA) 100 (KRUSS GmbH, Germany) was used to place the droplets on the powder surface and measure the resultant contact angle. Each measurement was repeated 25 times for each powder due to the possible complications in contact angle measurement of powders, such as powder between the droplet and camera obscuring the true contact angle, described above. The values stated are the mean of all measurements. An example DSA image is shown in Figure 4.

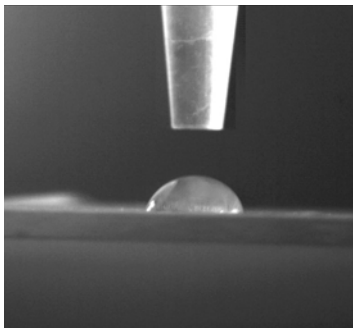

Figure 4: Example sessile drop sat on a powder bed

Slurryability Measurement

Slurryability was measured in a 5 L cylindrical stirred vessel with the geometric configuration that was found previously to incorporate powder most effectively into high concentration slurries[5,6]. This geometry is shown in Figure 5[6] and comprised a stainless steel flat-bottomed cylindrical mixing vessel with diameter, T = 0.17 m, a down-pumping pitched blade turbine (PBT) impeller with a diameter, D, of 0.085 m (D/T = 0.5). Off-bottom clearance, C, (measured to the middle of the impeller) was 0.085 m (C/T = 0.5; C = D). The impeller was placed off-centre, E, by 0.1 T (0.017 m) and tilted, α, by 10°. No baffles were used. The impeller speed, N, was fixed at 450 RPM.

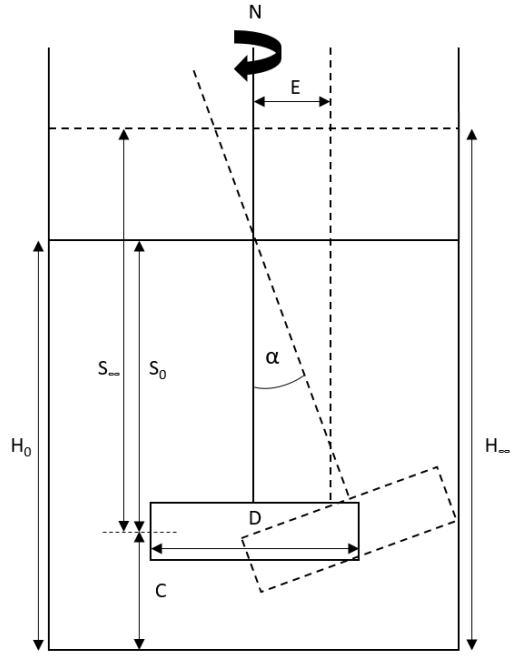

Figure 5: Mixing vessel schematic[6]

Slurryability was assessed by measuring the time taken to add 50 wt% powder to a given vessel. Prior to the start of the experiment the vessel with filled with 3.86 L of water and 3.86 kg of powder was weighed out into fifty × 77 g aliquots using a KTron KT20 loss in weight powder feeder configured to deliver a constant total mass. This allowed tracking of the amount of powder added to the vessel with time. The powder was added to water the stirred vessel described above up to 50

wt% as quickly as possible, adding each subsequent aliquot to the liquid surface as soon as the previous powder had been drawn down and incorporated into the slurry. The time and energy required to prepare a 50 wt% slurry was measured in this way for all powders studied. The slurryability of each powder was measured three times, the values used are the mean of these repeats.

The impeller shaft torque was measured using a calibrated Binsfield TorqueTrak 10k wireless strain gauge. The impeller power, P, was found from the shaft torque, Γ, as:

$$P = 2\pi N\Gamma \#(8)$$

The measured torque, and so impeller power draw was found to fluctuate by ±5 % of the reading value. All values used are the moving average value recorded over 1 s at a sampling frequency of 10 Hz.

Multivariate Analysis

Multivariate data analysis was carried out using JMP statistical software (SAS Institute Inc., UK). The data were first normalised using Z-score normalisation (or auto-scaling) as the different properties measured all have different units and scales. Z-score normalisation centres all the data around 0, with a standard deviation of 1 and is done simply by applying the following to all measurements:

$$Z_{i,m} = \frac{x_{i,m} - \bar{x}_i}{s_i} \#(9)$$

Where Z is the normalised value, x is the measurement of the ith property for the mth powder, $\bar{x}$ is the property mean for all powders, and s is the standard deviation of that property across all powders.

Principal component analysis is used as an exploratory tool to find trends and patterns within the dataset. PCA works by reducing the dimensionality of the dataset by orthogonal transformation, reducing the total number of variables to a set of orthogonal principal components (PC). The first PC

(PC1) describes the largest possible variance within the dataset, with subsequent PCs describing less variance with increasing dimensions. Each subsequent PC is orthogonal to all preceding PCs.

Partial Least Squares regression (PLS) works in a similar manner, reducing the number of dimensions in both the predictor (X) and response (Y) datasets into a series of orthogonal structures. The Y structures are then regressed onto the X structures to give a covariance matrix relating the two using a Nonlinear Iterative Partial Least Squares (NIPALS) algorithm. Leave-one-out cross-validation was used during this analysis. This involves calculating potential models whilst leaving out one of the observations (in this case leaving out a powder). The response, based on each model, is predicted for the left-out observation to give a residual between the predicted value and the measured value. This is repeated for all observations, giving a total precision value, given as the root mean squared error of cross validation (RMSECV). This is repeated testing a different number of latent variables in the two structures. The optimum number of structures is determined as that which gives the lowest RMSECV value, whilst explaining as much of the variation in the Y block as possible (in terms of R^2). VIP scores are then calculated using equation 3, shown above, to calculate the relative importance of each of the individual predictor variables studied.

PLS is a particularly effective technique for this application as it effective at handling co-correlation between predictor variables. This is important here due to the inevitable relationships between different powder properties. For example, as stated above, there is clearly a strong correlation between Hausner Ratio and Carr's Index. However, there will also be other significant related variables such as particle porosity and bulk density, many of the various dynamic flow properties, and particle size values and pressure drop measurements.

PLS models can be improved by removing noise in the original dataset. VIP scores can be used as a variable selection method to indicate which of the initial variables are likely to contribute only noise, and which contribute useful variance. Therefore, the PLS algorithm is run over the dataset twice. Once to find an initial model, calculating VIP scores of all variables. Insignificant variables (those

with a VIP score < 1) are then removed from the dataset and the model rebuilt. This will provide an improved model, with less overfitting[49].

The performance of the predictive models built using PLS can be considered by calculating the root mean square error (RMSE) between the predicted and measured values of slurryability. RMSE is calculated as:

$$RMSE = \sqrt{\frac{1}{N}\sum_{i=1}^{N}\left(Slurryability_{measured,i} - Slurryability_{Predicted,i}\right)^2} \quad \#(10)$$

Where N is the number of powders studied.

In order to validate the models built using partial least squares regression analysis two extra powders were studied, a zeolite material (zeolite 1) and another mixed oxide (mixed oxide 3). These powders were not included in the training sets used to build the models and so are used to study the applicability of the models outside of the original training set of powders.

Results and Discussion

Powder Characterisation

Table 1 gives the particle size, bulk density, skeletal density, and pore volume measurements for each of the thirteen powders studied in the training dataset. These powders were chosen to give a wide range of properties, as shown for all of these measures in Table 1.

Figure 6 shows the shear cell measurements at an initial consolidation stress of 15 kPa. The flow function coefficient is used to characterise how easily a powder will flow, with larger flow functions indicating easier flow, as shown in Figure 2. The glass frit showed the highest flow function coefficient, indicating it is the best flowing powder. The various alumina powders studied generally showed the lowest flow function values. The glass frit also showed the highest cohesion, with the

magnesia powders and mixed oxides also showing reasonable cohesion. Again, the alumina powders showed the lowest cohesion values.

Figure 7 shows the basic flow energies and aeration energies of the initial 13 powders studied. The glass frit and mixed oxide 1 required the most energy to flow, whereas the titania powder sample required the least. Many of the powders were found possible to fully aerate during the test, with the glass frit, mixed oxides, and γ-alumina 2 being the only powders where it was not possible. This meant that most of the powders showed a significant aeration index as the energy required to make them flow dropped considerably when they were fully aerated.

Figure 8 shows the compressibility and pressure drop measurements from the Freeman FT4 powder rheometer. The magnesia and titania proved to be the most compressible, with the mixed oxides and alumina powders showing little tendency to compress.

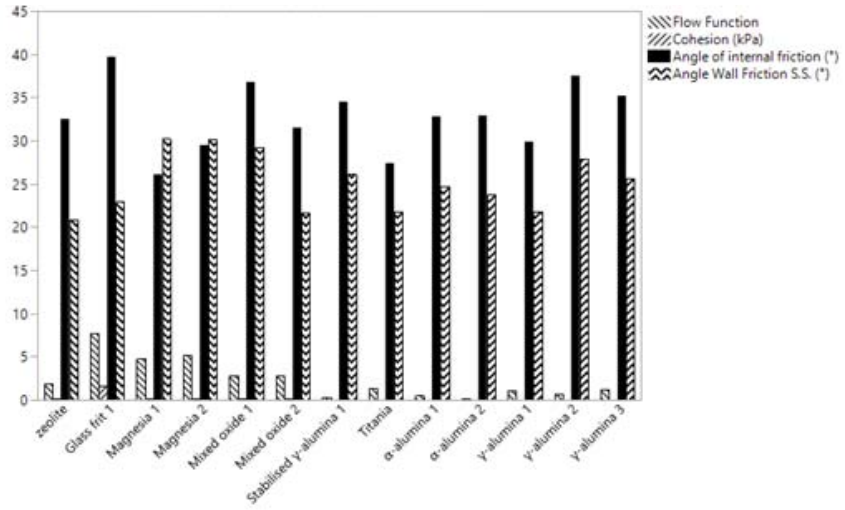

Figure 6: Shear cell measurements for initial 13 powders

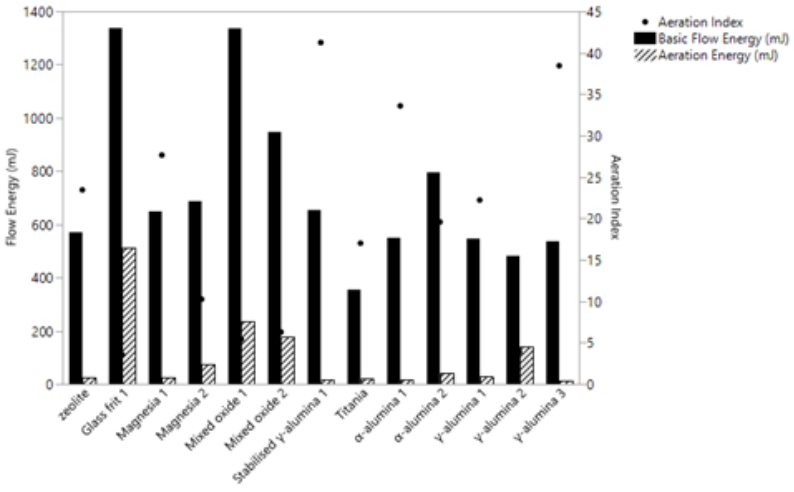

Figure 7: Basic flow energy and aeration energy test results from the Freeman FT4 for initial 13 powders

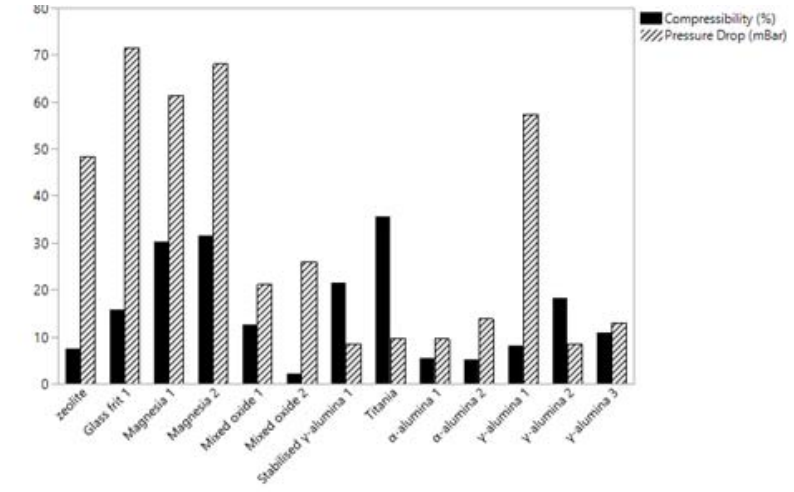

Figure 8: Compressibility and pressure drop tests from the Freeman FT4 for the initial 13 powders

Slurryability and powder ranking

In order to model the effect of powder and particle properties on the slurryability of a powder, a definition of powder slurryability is required that allows direct comparison between powders. The slurryability of a powder is defined in three ways:

1. t_{50} The time required to prepare a 50 wt% slurry.

2. E_{50} The cumulative specific energy required to prepare a 50 wt% slurry.
3. X_{11} The solid content at which it requires more than 1 kJ to raise the slurry solid content by 1 wt%.

These three approaches are shown graphically for three example powders in Figure 9, Figure 10, and Figure 11 respectively. Figure 9 shows the time taken to add powder to the vessel up to the final solid concentration of 50 wt%. t_{50} is defined as the time value of the final point of the curve. Figure 10 shows the cumulative energy required to incorporate powder into slurry. This energy is calculated using the measured impeller torque and mixing time. E_{50} is defined as the cumulative energy value of the final point of the curve. Figure 11 shows how this energy requirement increases with increasing solid content and defines X_{11} as the solid content when the curve for each powder crosses 1000 J $\%^{-1}$.

All three measures show a significant reduction in the slurryability of the powders considered as the solid content is increased, as seen by a turning point in all curves. These turning points align with the step change in incorporation performance that occurs as the solid concentration increases and the mechanism of incorporation changes as noted previously [5,6].

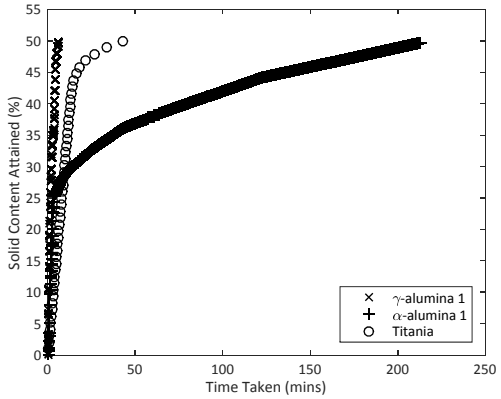

Figure 9: Slurryability approach 1 – time taken to prepare a 50 wt% slurry

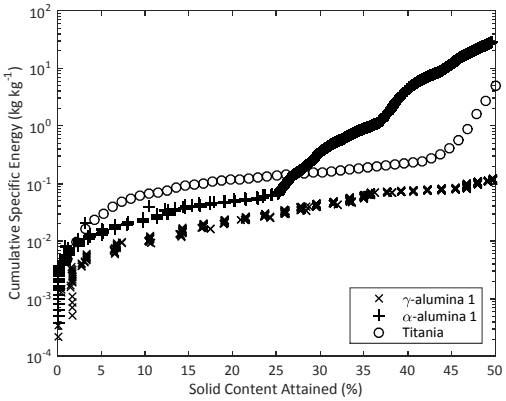

Figure 10: Slurryability approach 2 – total energy required to achieve a 50 wt% slurry

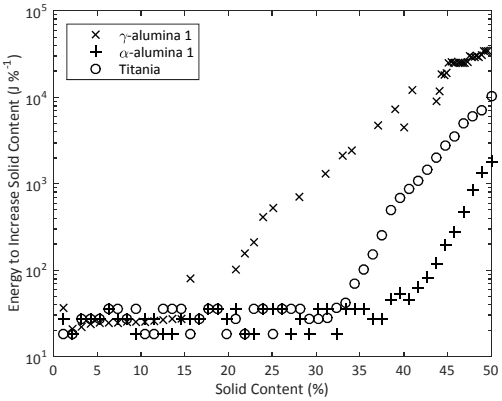

Figure 11: Slurryability approach 3 – solid content at which it requires at least 1 kJ to raise the solid content of the slurry by 1 wt%

Table 2

~~Table 2~~ shows the slurryability measurements for each of the thirteen initial powders. There was a significant range in powder slurryability within the dataset with slurry time to prepare a 50 wt% slurry at 6 minutes for the easiest powders (γ-alumina 1 and Mixed oxide 1) and over four hours for the least slurryable powder studied (Stabilised γ-alumina 1).

Table 2: Measured slurryability values

Powder Name	**Slurry Time (mins)**	**Slurry Energy (kJ kg^{-1})**	**Threshold Concentration (wt %)**
Mixed oxide 1	6.2	0.12	48.2
γ-alumina 1	6.0	0.11	48.8
α-alumina 1	212.0	28.2	32.1
α-alumina 2	171.3	22.4	38.2
Stabilised γ-alumina 1	250.0	34.5	25.1
Titania	92.6	9.9	41.3
Magnesia 1	7.1	0.25	47.3
Magnesia 2	75.5	1.2	41.5
Glass frit 1	21.3	1.3	46.2
Mixed oxide 2	8.1	0.8	47.6
Zeolite	15.1	0.21	45.2
γ-alumina 2	131.2	17.8	39.2
γ-alumina 3	21.8	3.2	43.2

Figure 12 shows the relative rankings of each powder in terms of their slurryability ranked from most easily incorporated to most difficult for each of the three measures of slurryability described above. It is clear that for most cases all three metrics give similar rankings of each powder.

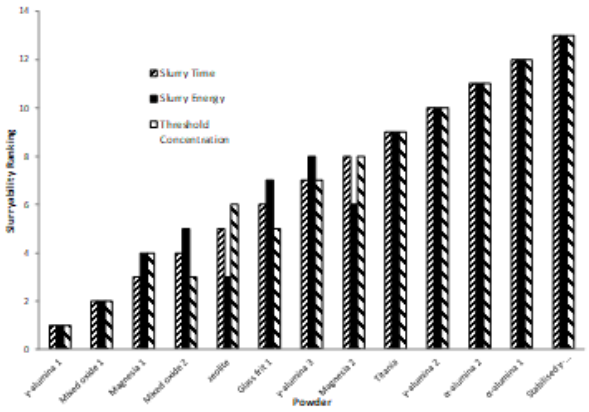

Figure 12: Relative rankings of each powder in terms of each slurryability measure with 1 being slurry time, 2 slurry energy, and 3 threshold concentration

Univariate Analysis

The most likely powder properties governing how easy a powder is to incorporate are the volume concentration and the interfacial tension with the liquid into which the powder is being added. Each of these can be studied in isolation.

Powder Density

Figure 11 shows the energy to increase the solid content of three slurries by 1 wt% of three powders with different slurryabilities as their solid content by weight is increased. Figure 13 shows the same three powders with the slurry solid contents expressed by volume. The two alumina powders appear to behave similarly when normalised by their volume, with their X_{11} occurring at around 50 vol% for both powders. However, the titania powder does not, reaching a considerably higher solid content of 71 vol% before it requires 1 kJ to add an addition 1 wt% of powder.

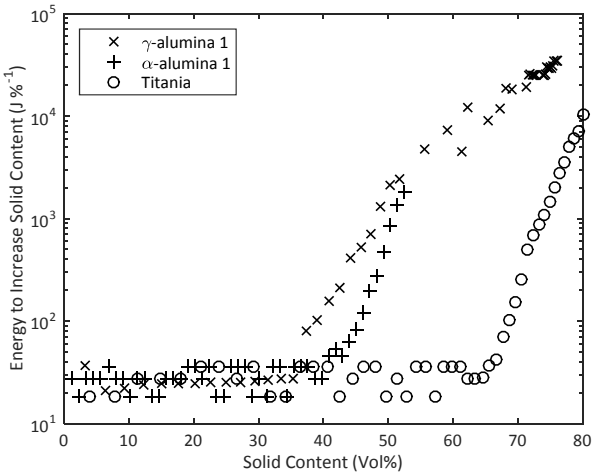

Figure 13: Energy to increase the solid content slurry by 1 wt% against the slurry solid volume concentration

Contact angle

Figure 14 shows the measured three phase contact angle plotted against the threshold slurry content slurryability measure. It is clear there is little trend between the contact angle with water and the slurryability of a powder, indicating that the interfacial tension between the solid and the

liquid has little effect in how easy that powder is to incorporate. However, given that measuring the contact angle for porous powders is notoriously difficult, it is it is difficult to draw a firm conclusion. An improvement to this study would be to repeat this measurement using a number of different liquids, with a wide range of dispersive and polar surface tension components to find the solid surface free energy for each powder, as described by Owens, Wendt, Rabel, and Kaelbe[50–52].

It is clear that, although some differences in slurryability can be explained when looking at properties in isolation, there will always be exceptions. This is because the system being studied is complex and cannot be described by a single property. Therefore, a multivariate approach is needed.

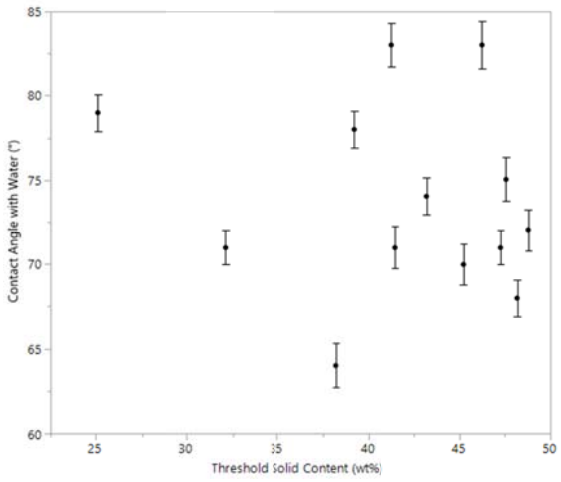

Figure 14: Three phase contact angles with water for initial 13 powders measured using a KRUSS DSA 100

Multivariate analysis

Principal Components Analysis (PCA)

Figure 15 shows a PCA scores plot for the first two principal components within the dataset, explaining the relationships between the samples in the first two principal components. Powders that are similar will be clustered in multivariate space, visualised by their similar score values. These first two components account for 58.6 % of the variation measured within the powder properties, with 74.3 % of the variation described by three principal components, and adding more principal

components beyond three describes relatively little extra variation for each PC added. This suggests that three principal components are required to suitably describe the measured variation between the powders, with the first two describing the majority of the variation. It is interesting to note that the different mixed oxides, magnesia, and α-alumina powders are clustered with one another in pairs, suggesting that these pairs are similar powders. The most unique powder of all appears to be the glass frit, which sits by itself with a high value in PC1.

Figure 16 shows the loadings plot of each of the measured powder properties. In the loadings plot, points close together suggest correlation whereas points in opposite quadrants (i.e. directly opposite one another through the centre of the plot) show anti-correlation. Points in adjacent quadrants show little or no correlation to one another. This is demonstrated clearly by the three slurryability measures, where slurry time and slurry energy are closely correlated and strongly anticorrelated to the threshold concentration (which responds in the opposite direction to slurry time and energy as powders become harder to incorporate). Some powder properties clearly cluster into sensible groups. For example particle size measurements cluster together with the pore volume, showing correlation, as do the Carrs Index and Hausner Ratio. Many of these are expected, as mentioned previously, showing strong co-correlation between measured variables. The angle of wall friction, powder flow function, and powder compressibility show little correlation with any other parameter. It is important to consider the standard deviation as well as the mean because more variable powders may behave differently than consistent powders, something not described by the mean value alone. However, most standard deviation and mean values appear strongly correlated due to their close proximity in
Figure 16. This is likely because the value of the standard deviation is likely to scale in magnitude with the mean.

It is interesting to note the lack of correlation between the D_{10} and D_{50} values with the D_{90} values. This is likely because the PSD is being normalised by volume, where a single large particle can contain a significant amount of the measured volume, having a particularly strong influence on the value of D_{90} but not on either the D_{50} or D_{10}. This is most strongly seen in the glass frit powder, which has the lowest D_{10} and D_{50} values of all powders studied but the highest D_{90} value.

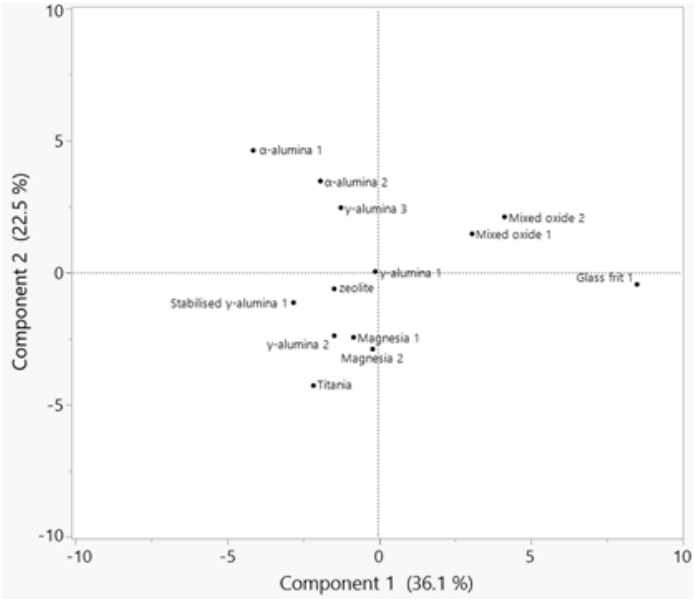

Figure 15: PCA scores plot

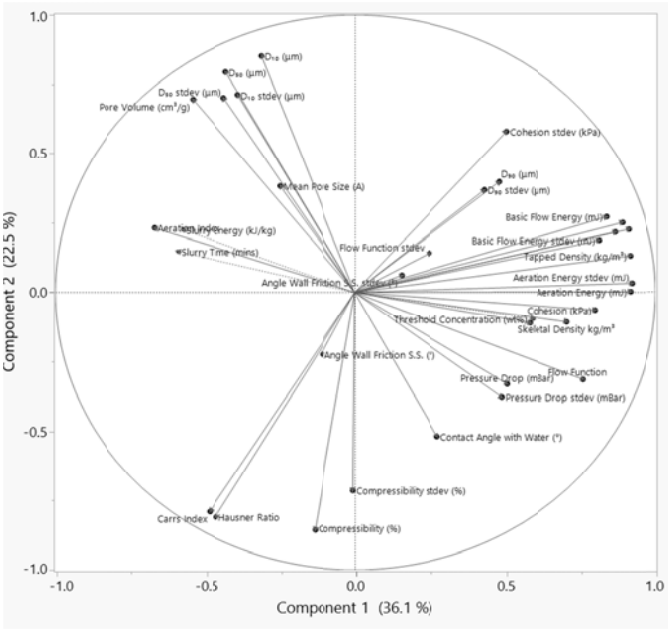

Figure 16: Loadings plot for first two principal components

Partial Least Squares (PLS)

Partial least squares regression modelling was applied to the entire training dataset of 13 original powders. This included 34 predictor variables, when factoring in both the mean and standard deviation values for repeats for each of the characterisation tests described above.

Initially a NIPALS PLS algorithm was carried out with two latent variables, the number of latent variables giving the smallest RMSECV value during validation. Figure 17 shows the VIP scores for all variables in this initial PLS model, VIP scores of <1 are considered insignificant within the model. The standard deviations for most predictors are unimportant in the model, this is because (as seen in Figure 16) they are strongly correlated with their corresponding means and so do not have additional significant contribution to the PLS models. The powder compressibility, wall friction angle with stainless steel, and Hausner ratio and Carrs Index are all also unimportant in the model. This is understandable as the powder is not in contact with a wall unless at the free liquid surface in the vessel and there is little compression of the powder during decanting and pouring onto the liquid surface.

The most significant variables in the projection include the pore volume, pressure drop test result, bulk densities, and powder cohesion. The plots in Figure 18 show the measured versus predicted values in terms of all three slurryability measures from this model. Slurry time and slurry threshold concentration show reasonable agreement at this stage, although there is clearly still error in the predictions. The prediction of the slurry energy does not show a strong correlation with actual measured values. In all three models the magnesia 2 powder is the least well predicted of all powders in the model. The VIP scores in Figure 17 can be used to inform the choice of which parameters can be removed to create a new model, with less inherent noise in the predictor dataset. This is done by rerunning the PLS NIPALS algorithm but only considering the variables with a VIP score greater than one in the original model (i.e. those larger than the blue threshold line in Figure 17).

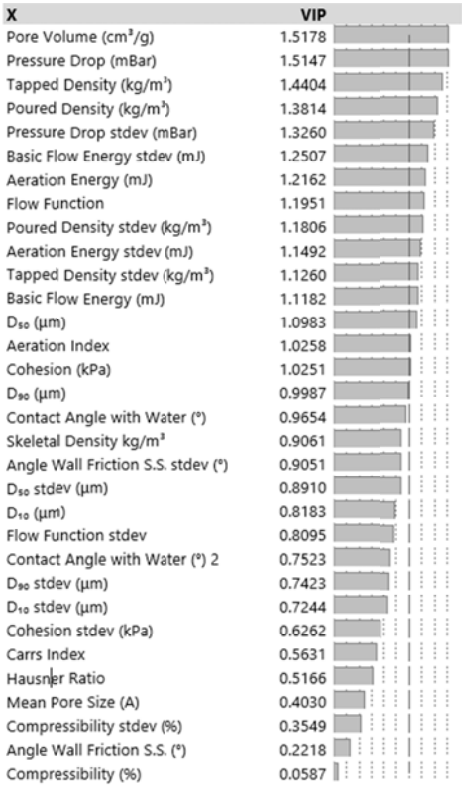

X	VIP
Pore Volume (cm^3/g)	1.5178
Pressure Drop (mBar)	1.5147
Tapped Density (kg/m^3)	1.4404
Poured Density (kg/m^3)	1.3814
Pressure Drop stdev (mBar)	1.3260
Basic Flow Energy stdev (mJ)	1.2507
Aeration Energy (mJ)	1.2162
Flow Function	1.1951
Poured Density stdev (kg/m^3)	1.1806
Aeration Energy stdev (mJ)	1.1492
Tapped Density stdev (kg/m^3)	1.1260
Basic Flow Energy (mJ)	1.1182
D_{50} (µm)	1.0983
Aeration Index	1.0258
Cohesion (kPa)	1.0251
D_{90} (µm)	0.9987
Contact Angle with Water (°)	0.9654
Skeletal Density kg/m^3	0.9061
Angle Wall Friction S.S. stdev (°)	0.9051
D_{50} stdev (µm)	0.8910
D_{10} (µm)	0.8183
Flow Function stdev	0.8095
Contact Angle with Water (°) 2	0.7523
D_{90} stdev (µm)	0.7423
D_{10} stdev (µm)	0.7244
Cohesion stdev (kPa)	0.6262
Carrs Index	0.5631
Hausner Ratio	0.5166
Mean Pore Size (A)	0.4030
Compressibility stdev (%)	0.3549
Angle Wall Friction S.S. (°)	0.2218
Compressibility (%)	0.0587

Figure 17: Table for VIP scores for all variables in initial PLS model with two latent variables

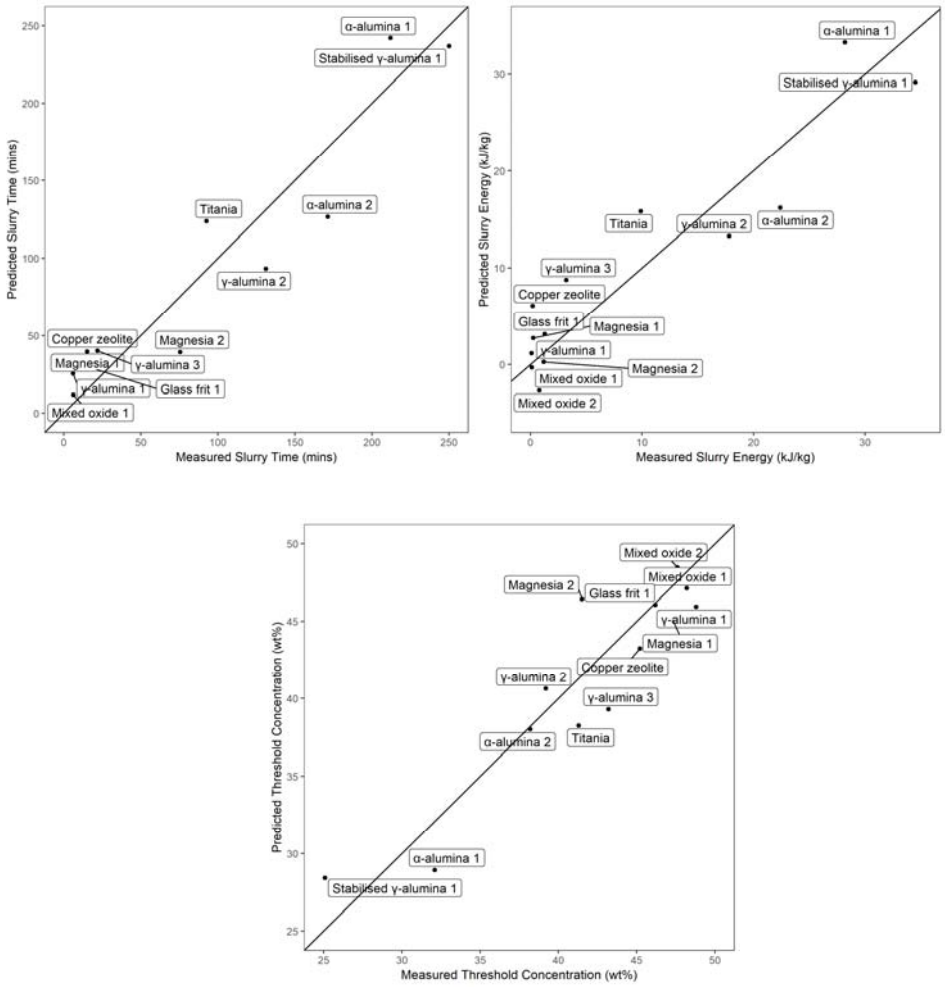

Figure 18: Measured vs predicted slurryability values in terms of slurry time (a), slurry energy (b), and threshold concentration (c) for initial PLS model

The resultant VIP scores for the new model are shown in Figure 19. The pore volume and pressure drop measurements remain the most significant parameters, with high importance still given to the bulk density measurements. In this new model, most of the bulk powder flow measurements, such as flow function, basic flow energy, aeration energy, and aeration index drop below the VIP significance threshold of 1.

Figure 20 shows the predictive performance of this new model for the three measures of slurryability. The prediction for the threshold concentration measure gives a strong performance for

all powders studied. The slurry energy prediction also shows strong performance, although some of the very easiest to incorporate slurries show less strong predictions. The slurry time predictive performance is weaker than the other two. This is, again, most evident amongst the easiest to incorporate slurries, with magnesia 1 predicted as having a negative slurry time, which is obviously unrealistic. Table 3 shows RMSE values for both models, showing the error between measured and predicted slurryability values. As described above, the predictive performance improves when noise is removed in the second model for both the slurry energy and threshold concentration measurements. However, the slurry time predictive performance drops.

X	VIP
Pore Volume (cm^3/g)	1.1834
Pressure Drop (mBar)	1.1303
Aeration Energy (mJ)	1.0905
Tapped Density (kg/m^3)	1.0570
Pressure Drop stdev (mBar)	1.0527
Poured Density (kg/m^3)	1.0385
Cohesion (kPa)	1.0178
D_{50} (µm)	1.0134
Poured Density stdev (kg/m^3)	0.9620
Basic Flow Energy stdev (mJ)	0.9603
Aeration Energy stdev (mJ)	0.9406
Basic Flow Energy (mJ)	0.9295
Flow Function	0.9100
Tapped Density stdev (kg/m^3)	0.9047
Aeration Index	0.7231

Figure 19: Table for VIP scores for all variables in second PLS model with three latent variables

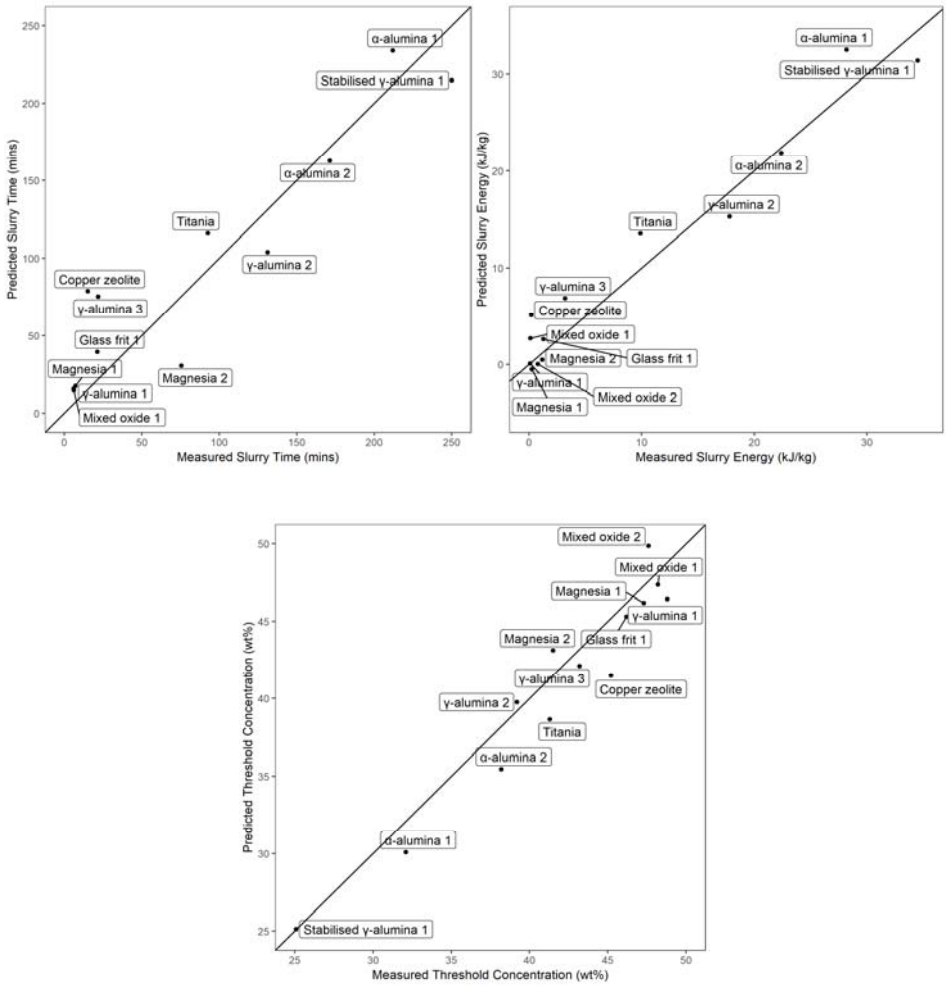

Figure 20: *Measured vs predicted slurryability values in terms of slurry time (a), slurry energy (b), and threshold concentration (c) for second PLS model*

Table 3: *RMSE values for the two models*

	Slurry time	Slurry energy	Threshold concentration
Initial model RMSE	26.6	4.28	2.64
Second model RMSE	33.4	2.72	1.96

The VIP scores in Figure 17 show the key powder properties that affect how easily the powder may be incorporated. The four most important properties are the pore volume, pressure drop, aeration

energy, and bulk density. Knowing this, it is possible to hypothesise some physical meaning behand why these properties are important.

As described above, the powder content is described in weight fraction as this is the easiest to measure and matches formulation specifications. However, volume concentration of the dispersed phase(s) is important in the behaviour of any multiphase system. This makes explaining the importance of the powder bulk density trivial, as powders with low bulk densities will ostensibly occupy a larger volume for the same weight content as powders with higher densities. This is clearly shown as powders with low bulk densities such as the titania, stabilised γ-alumina, and α-alumina 1 proved to be some of the hardest to incorporate powders, based on their slurryability measures shown in Table 2.

The significance of pore volume is also relatively simple to explain, as particles with significant porosity are likely to occupy a larger volume until the pores fully fill with liquid. This means the particle will act as a less dense particle initially. The presence of air inside the particle is also likely to increase the buoyancy force on the particle as it hits the liquid surface when initially added to the vessel. This increased buoyancy force will make it harder to draw the powder down into the fluid and incorporate it into a slurry. The presence of pores also generates the possibility of a dynamic effect to occur, where even after the particles are incorporated, whilst the pores are still filling with liquid they occupy a larger volume in the slurry. This gives a temporarily higher solid phase volume concentration, increasing the slurry apparent viscosity and making it more difficult to add additional powder until the air inside the pores has been displaced. This effect is described by Wood *et al*[5].

The importance of the aeration energy and pressure drop measurements in the models is slightly harder to explain physically. However, as the powder is poured onto the liquid surface, it is possible that less aeratable powders have a tendency to cluster as they are poured and aerated. The consequence of this is that as the powder hits the liquid surface and begins to wet, clustered particles are more likely to form semi-wet agglomerates on the free surface. Wood *et al*[5] showed

that formation of large agglomerates on the free surface was one of the main hindrances to increasing the solid content of a concentrated slurry.

Figure 16 shows that the pressure drop measurements are strongly anti-correlated with D_{10} and D_{50} values. The Kozeny-Carman equation indicates pressure drop is dominated by bed voidage and specific surface area. Wide size distributions will lead to lower voidages while increasing amounts of fines will lead to higher surface area; both of which contribute to an increase in pressure drop. It is apparent therefore that the presence of fine particles has a strong negative impact on the slurryability of a powder as the extra surface they provide increases the complexity of the slurry rheology. The presence of these fine particles may well be seen more effectively by measurements of low permeability than in volume weighted particle size distribution (light scattering-based) measurements, explaining why pressure drop and not D_{10} is significant in the models.

Model Validation

Another mixed oxide powder and a zeolite material not included in the original training set of 13 powders were studied to assess the applicability of this PLS model beyond outside of the original data set and provide validation of the PLS model. The results from measurements of the identified key parameters for these powders are shown in Table 4.

Table 4: Relevant properties of the two validation powders studied

Property	Zeolite 1	Mixed oxide 3
D_{50} (µm)	33.2	60.4
Poured Density (kg m^{-3})	443.2	943.5
Tapped Density (kg m^{-3})	394.6	799.6
Cohesion (kPa)	0.121	0.095
Aeration Energy (mJ)	4.2	17.3
Pressure Drop (mBar)	10.3	29.6
Pressure Drop stdev (mBar)	3.54	7.21
Pore Volume (cm^3 g^{-1})	0.842	0.302

Figure 21 shows the plots from Figure 20 with these two validation powders added. In absolute terms all three slurryability metrics are well predicted, lying close to the measured = predicted line.

Table 5 shows absolute and percentage error for both validation powders for all three metrics. The mixed oxide 1 powder showed high percentage error for both slurry time and energy, although this is because it is amongst the easiest to incorporate powders, where slurry time and energy requirements are low and so small absolute errors give large percentage errors. The threshold concentration slurryability is well predicted for both powders, with an error of less than ±10 %.

Table 5: Absolute and percentage error in predictions for the two validation powders

Powder	Slurry time error		Slurry energy error		Threshold concentration error	
	Absolute (mins)	Percentage (%)	Absolute (kJ kg^{-1})	Percentage (%)	Absolute (wt%)	Percentage (%)
Mixed oxide 1	11.3	77.3	0.7	99.2	2.3	5.3
Zeolite 1	-27.3	-16.3	-2.4	-12.4	2.9	-8.6

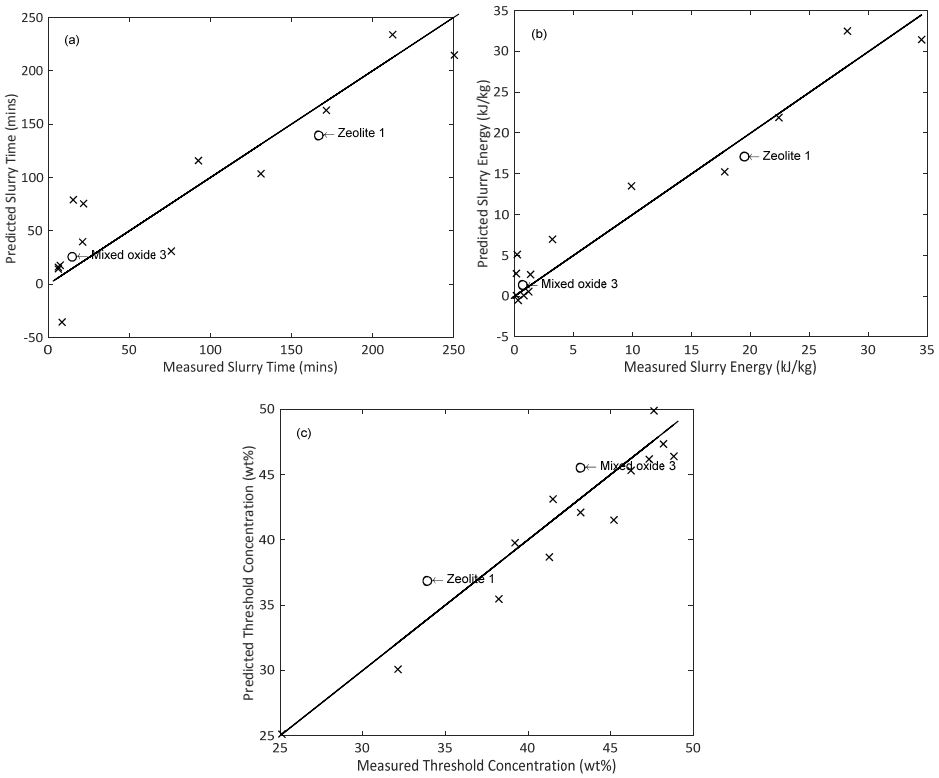

Figure 21: Measured vs predicted slurryability values for two validation powders in terms of slurry time (a), slurry energy (b), and threshold concentration (c) for second PLS mode

Conclusions

This study has used multivariate statistical modelling techniques to elucidate the most significant powder properties determining how easily a given powder may be incorporated into a high solid content slurry in a stirred vessel. The ease with which a powder is incorporated into a slurry is defined here as the *slurryability* of the powder and is measured in three distinct ways: firstly, the time required to achieve a 50 wt% solid content slurry in a fixed vessel geometry configuration, secondly the energy required to achieve the same. The third metric considered is a threshold slurry concentration at which it requires more than 1 kJ to increase the solid content by a further 1 % in the vessel studied.

Partial least squares models are built which predict the slurryability of a powder based on its key properties. The most significant properties, based on variable importance in projection scores, are the particle pore volume, the pressure drop result of the Freeman FT4 powder rheometer permeability test, the powder aeration energy, again measured on the Freeman FT4 powder rheometer, powder tapped and poured density, and the d_{50} particle size of the powder. By measuring these six properties it is shown to be possible to predict the slurryability of two validation powders, not present in the original training dataset, to an error in threshold concentration of ±10 %.

Acknowledgements

Thomas Wood is funded by the EPSRC Centre for Doctoral Training in Formulation Engineering at the University of Birmingham (EPSRC grant number EP/L015153/1) and Johnson Matthey.

References

1. Braun JH, Baidins A, Marganski RE. TiO2 pigment technology: a review. *Prog Org Coat*. 1992;20(2):105-138.

2. Nowak E, Robbins P, Combes G, Stitt EH, Pacek AW. Measurements of contact angle between fine, non-porous particles with varying hydrophobicity and water and non-polar liquids of different viscosities. *Powder Technol*. 2013;250:21-32.

3. Fleming SE, Sosulski FW, Kilara A, Humbert ES. Viscosity and Water Absorption Charactercstics of Slurries of Sunflower and Soybean Flours, Concentrates and Isolates. *J Food Sci*. 2006;39(1):188-192.

4. Chou K-S, Lee L-J. Effect of Dispersants on the Rheological Properties and Slip Casting of Concentrated Alumina Slurry. *J Am Ceram Soc*. 2005;72(9):1622-1627.

5. Wood T, Simmons MJH, Greenwood RW, Stitt EH. Concentrated slurry formation via drawdown and incorporation of wettable solids in a mechanically agitated vessel. *AIChE J*. 2018;64(5):1885-1895.

6. Wood T, Simmons MJH, Stitt EH. Optimisation of stirred vessel geometry for the drawdown and incorporation of floating solids to prepare concentrated slurries. *Chem Eng Res Des*. 2018;133:70-78.

7. Prescott JK, Barnum RA. On powder flowability. *Pharm Technol*. 2000;24:60-85.

8. Vasilenko A, Glasser BJ, Muzzio FJ. Shear and flow behavior of pharmaceutical blends — Method comparison study. *Powder Technol*. 2011;208(3):628-636.

9. Carr RL. Evaluating flow properties of solids. January 1965.

10. e Silva JPS, Splendor D, Gonçalves IMB, Costa P, Sousa Lobo JM. Note on the Measurement of Bulk Density and Tapped Density of Powders According to the European Pharmacopeia. *AAPS PharmSciTech*. 2013;14(3):1098-1100.

11. Hausner HH. FRICTION CONDITIONS IN A MASS OF METAL POWDER. *Int J Powder Met 3 No 4 7-13Oct 1967*. January 1966.

12. Krieger IM, Dougherty TJ. A Mechanism for Non-Newtonian Flow in Suspensions of Rigid Spheres. *Trans Soc Rheol*. 1959;3:137-152.

13. Koynov S. Using statistical methods to optimize powder flow measurements and to predict powder processing performance. 2015.

14. Chilekar VP, Schaaf J van der, Kuster BFM, Tinge JT, Schouten JC. Influence of elevated pressure and particle lyophobicity on hydrodynamics and gas–liquid mass transfer in slurry bubble columns. *AIChE J*. 2009;56(3):584-596.

15. Ruthiya KC, van der Schaaf J, Kuster BFM, Schouten JC. Similar effect of carbon and silica catalyst support on the hydrogenation reaction rate in organic slurry reactors. *Chem Eng Sci*. 2005;60(22):6492-6503.

16. Buckton G. The assessment, and pharmaceutical importance, of the solid/liquid and the solid/vapour interface: a review with respect to powders. *Int J Pharm*. 1988;44(1):1-8.

17. Binks BP, Whitby CP. Nanoparticle silica-stabilised oil-in-water emulsions: improving emulsion stability. *Colloids Surf Physicochem Eng Asp*. 2005;253(1):105-115.

18. Dickinson E. Use of nanoparticles and microparticles in the formation and stabilization of food emulsions. *Trends Food Sci Technol*. 2012;24(1):4-12.

19. Dickinson E. Food emulsions and foams: Stabilization by particles. *Curr Opin Colloid Interface Sci*. 2010;15(1):40-49.

20. Young T. An Essay on the Cohesion of Fluids. *Philos Trans R Soc Lond*. 1805;95:65-87.

21. Yan N, Maham Y, Masliyah JH, Gray MR, Mather AE. Measurement of Contact Angles for Fumed Silica Nanospheres Using Enthalpy of Immersion Data. *J Colloid Interface Sci*. 2000;228(1):1-6.

22. Voelkel A, Strzemiecka B, Adamska K, Milczewska K. Inverse gas chromatography as a source of physiochemical data. *J Chromatogr A*. 2009;1216(10):1551-1566.

23. Washburn EW. The Dynamics of Capillary Flow. *Phys Rev*. 1921;17(3):273-283.

24. Dang Vu T, Jan H. Characterization of porous materials by capillary rise method. *Physicochem Probl Miner Process*. 2005;39.

25. Galet L, Patry S, Dodds J. Determination of the wettability of powders by the Washburn capillary rise method with bed preparation by a centrifugal packing technique. *J Colloid Interface Sci*. 2010;346(2):470-475.

26. Kirdponpattara S, Phisalaphong M, Newby BZ. Applicability of Washburn capillary rise for determining contact angles of powders/porous materials. *J Colloid Interface Sci*. 2013;397:169-176.

27. Kirchberg S, Abdin Y, Ziegmann G. Influence of particle shape and size on the wetting behavior of soft magnetic micropowders. *Powder Technol*. 2011;207(1):311-317.

28. Nowak E, Combes G, Stitt EH, Pacek AW. A comparison of contact angle measurement techniques applied to highly porous catalyst supports. *Powder Technol*. 2013;233:52-64.

29. Marmur A. Equilibrium contact angles: theory and measurement. *Colloids Surf Physicochem Eng Asp*. 1996;116(1–2):55-61.

30. Pearson K. LIII. On lines and planes of closest fit to systems of points in space. *Lond Edinb Dublin Philos Mag J Sci*. 1901;2(11):559-572.

31. Ince H, Trafalis TB. Kernel principal component analysis and support vector machines for stock price prediction. *IIE Trans*. 2007;39(6):629-637.

32. Naidu DV, Raol JR. Pixel-level Image Fusion using Wavelets and Principal Component Analysis. *Def Sci J*. 2008;58.

33. Bohidar NR, Restaino FA, Schwartz JB. Selecting key parameters in pharmaceutical formulations by principal component analysis. *J Pharm Sci*. 1975;64(6):966-969.

34. Wang Y, Li T, Muzzio FJ, Glasser BJ. Predicting feeder performance based on material flow properties. *Powder Technol*. 2017;308:135-148.

35. Wold S, Sjöström M, Eriksson L. PLS-regression: a basic tool of chemometrics. *Chemom Intell Lab Syst*. 2001;58(2):109-130.

36. Caporaso N, Whitworth MB, Fowler MS, Fisk ID. Hyperspectral imaging for non-destructive prediction of fermentation index, polyphenol content and antioxidant activity in single cocoa beans. *Food Chem*. 2018;258:343-351.

37. Haaland DM, Thomas EV. Partial least-squares methods for spectral analyses. 1. Relation to other quantitative calibration methods and the extraction of qualitative information. *Anal Chem*. 1988;60(11):1193-1202.

38. Sjöblom J, Svensson O, Josefson M, Kullberg H, Wold S. An evaluation of orthogonal signal correction applied to calibration transfer of near infrared spectra. *Chemom Intell Lab Syst*. 1998;44(1):229-244.

39. Gurden SP, Martin EB, Morris AJ. The introduction of process chemometrics into an industrial pilot plant laboratory. *Chemom Intell Lab Syst*. 1998;44(1):319-330.

40. Wise BM, Gallagher NB. The process chemometrics approach to process monitoring and fault detection. *J Process Control*. 1996;6(6):329-348.

41. Tran TN, Afanador NL, Buydens LMC, Blanchet L. Interpretation of variable importance in Partial Least Squares with Significance Multivariate Correlation (sMC). *Chemom Intell Lab Syst*. 2014;138:153-160.

42. Schulze D. Powders and Bulk Solids. 2008.

43. Bharadwaj R, Ketterhagen WR, Hancock BC. Discrete element simulation study of a Freeman powder rheometer. *Chem Eng Sci*. 2010;65(21):5747-5756.

44. A. Alzaydi A. Flow of Gases through Porous Media. January 1975.

45. Carman PC. The determination of the specific surface of powders. *J Soc Chem Ind*. 1938;57:225-234.

46. Leturia M, Benali M, Lagarde S, Ronga I, Saleh K. Characterization of flow properties of cohesive powders: A comparative study of traditional and new testing methods. *Powder Technol*. 2014;253:406-423.

47. Drelich J, Miller JD, Hupka J. The Effect of Drop Size on Contact Angle over a Wide Range of Drop Volumes. *J Colloid Interface Sci*. 1993;155(2):379-385.

48. Kranias S. Effect of drop volume on static contact angles. *Kruus Appl Notes*. 2004:2.

49. Akarachantachote N, Chadcham S, Saithanu K. Cutoff threshold of variable importance in projection for variable selection. *Int J Pure Apllied Math*. 2014;94.

50. Kaelble DH. Dispersion-Polar Surface Tension Properties of Organic Solids. *J Adhes*. 1970;2(2):66-81.

51. Owens DK, Wendt RC. Estimation of the surface free energy of polymers. *J Appl Polym Sci*. 2003;13(8):1741-1747.

52. Rabel W. Einige Aspekte der Benetzungstheorie und ihre Anwendung auf die Untersuchung und Veränderung der Oberflächeneigenschaften von Polymeren. *Farbe Lacke*. 1971;77(10):997-1005.